AN X-RAY PHOTOELECTRON SPECTROSCOPY STUDY OF THE PRODUCTS OF THE INTERACTION OF GASEOUS IrF$_6$ WITH FINE UO$_2$F$_2$

by

Vladimir N. PRUSAKOV[1], Yury A. TETERIN[1], Nikolai M. TROTSENKO[1], Konstantin I. MASLAKOV[1], Anton Yu. TETERIN[2], Kirill E. IVANOV[1], Filipp S. BOCHAGIN[1], and Dmitry V. UTROBIN[1]

Nuclear fuel reprocessing by fluorination, a dry method of regeneration of spent nuclear fuel, uses UO$_2$F$_2$ for the separation of plutonium from gaseous mixtures. Since plutonium requires special treatment, IrF$_6$ was used as a thermodynamic model of PuF$_6$. The model reaction of the interaction of gaseous IrF$_6$ with fine UO$_2$F$_2$ in the sorption column revealed a change of color of the sorption column contents from pale-yellow to grey and black, indicating the formation of products of such an interaction. The X-ray photoelectron spectroscopy study showed that the interaction of gaseous IrF$_6$ with fine UO$_2$F$_2$ at 125 °C results in the formation of stable iridium compounds where the iridium oxidation state is close to Ir^{3+}. The dependence of the elemental compositions of the layers in the sorption column on the penetration depth of IrF$_6$ was established.

Key words: X-ray photoelectron spectroscopy, uranyl fluorite, iridium hexafluoride, technology of isolation of actinides from gas mixtures

INTRODUCTION

Nuclear fuel reprocessing by fluorination, a (dry) method of regeneration of spent nuclear fuel (SNF), uses uranyl fluorite (UO$_2$F$_2$) for the separation of plutonium from gaseous mixtures [1]. The Gibbs energy (G^0_{298}) of 74 kcal/mole for the suggested reactions of UO$_2$F$_2$ with PuF$_6$, unlike that of UO$_2$F$_2$ with UF$_6$ (51 kcal/mole), indicates a possible PuF$_6$ selectivity from the mixture (PuF$_6$, UF$_6$, F$_2$, N$_2$, and volatile fluorides) [2]. It has to be noted that the F$_2$ concentration can reach up to 25 vol.%. Therefore, the optimal temperature regime for the PuF$_6$ extraction on UO$_2$F$_2$ is, obviously, related to the F$_2$-UO$_2$F$_2$ interaction (G^0_{298} = –59 kcal/mole [2]). Experiments with pure fluorine were performed in order to establish temperature dependence on the UO$_2$F$_2$ + 2F$_2$ UF$_6$ + O$_2$ reaction rate. At 130 °C, the UO$_2$F$_2$ fluorination was slow. Since plutonium requires special treatment, IrF$_6$ was used as a thermodynamic model of PuF$_6$. This compound is as reactive and volatile as PuF$_6$. Experiments on the interaction of PuF$_6$ with UO$_2$F$_2$ have to be carried out and are scheduled for the nearest future.

An X-ray photoelectron spectroscopy (XPS) study of the samples of the products of the interaction of gaseous IrF$_6$ and fine UO$_2$F$_2$ was carried out in this work in order to study the possibility of the formation of stable compounds on the surface of uranyl fluoride granules, the distribution of these compounds along the sorption column and to determine iridium oxidation states. X-ray photoelectron spectroscopy is the most adequate method to solve these problems. It has been widely used to study compounds of various elements, including actinides [3-6].

Authors' addresses:
[1] Russian Research Centre "Kurchatov Institute"
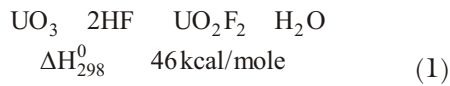   1, Kurchatov square, Moscow 123182, Russia
[2] N. S. Kurnakov Institute of General and Inorganic
    Chemistry of RAS, GSP-1,
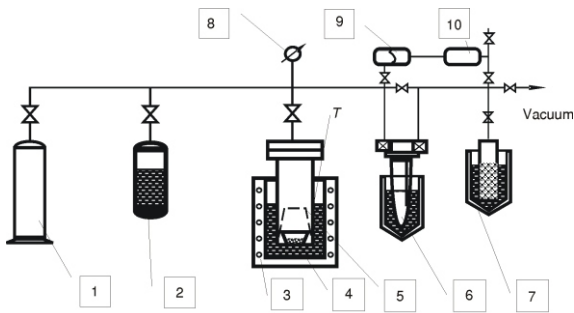   31, Leninsky Prospect, Moscow I-71, 119991, Russia

E-mail address of corresponding author:
prusakov@imp.kiae.ru (V. N. Prusakov)

EXPERIMENT

Uranyl fluoride (UO_2F_2) was prepared from the interaction of uranium trioxide (UO_3) with dry hydrogen fluoride (HF) as reaction (1) (ΔH_{298}^0 – standard enthalpy change of reaction):

$$UO_3 + 2HF \rightarrow UO_2F_2 + H_2O$$
$$\Delta H_{298}^0 = -46\,kcal/mole \qquad (1)$$

in the temperature range 100-150 °C. The diagram of the device is shown in fig. 1.

Figure 1. Diagram of the device for the synthesis of uranyl fluoride
1 – argon cylinder; 2 – container with hydrogen fluoride; 3 – furnace with oil bath; 4 – teflon (platinum) cup with UO_3; 5 – teflon hood; 6 – cooling trap; 7 – cooling coal trap; 8 – pressure-and-vacuum gage; 9 – differential manometer; 10 – buffer capacity

The reaction proceeds at a significant rate and with practically 100% yield. The crystallization water was removed in vacuum at about 150 °C. The photograph (fig. 2) shows UO_2F_2 after a long contact with water vapors (left) and after the removal of water
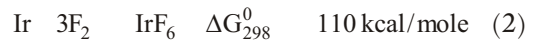

Figure 2. The photograph of UO_2F_2 after a long contact with water vapors (left) and after the removal of water (right)
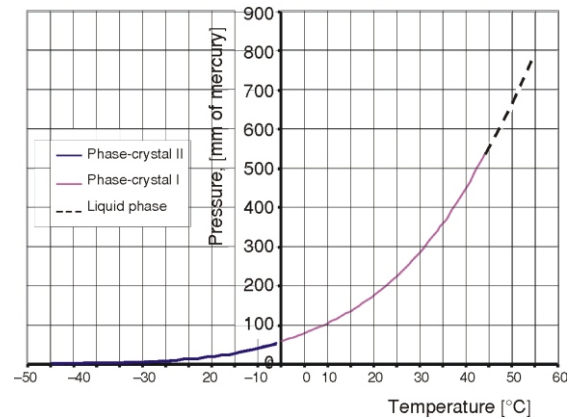
(right). The specific surface of UO_2F_2 measured with "Sorbi" by Brunauer-Emmett-Teller was 2.08 m²/g ± 0.07 m²/g. The porosity (ε%) and mean conditional size were measured by the program "Surch" to be 39% and 0.940 m, respectively.

Iridium hexafluoride (IrF_6) was synthesized from metallic iridium by fluorination under static conditions, according to the reaction (2) (ΔH_{298}^0 – standard Gibbs energy of IrF_6 formation):

$$Ir + 3F_2 \rightarrow IrF_6 \quad \Delta G_{298}^0 = -110\,kcal/mole \qquad (2)$$

IrF_6 melting temperature is 44.4 °C and boiling temperature is 53 °C. IrF_6 saturated vapor pressure *vs.* temperature is given in fig. 3. Solid IrF_6 is pale-yellow, liquid IrF_6 turns brown-yellow.

Figure 3. Saturated vapor pressure of iridium hexafluoride [2]
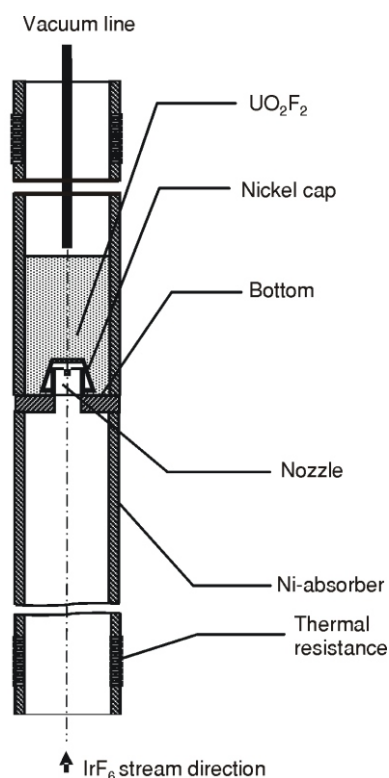*Before –1 °C – phase-crystal II; from –0.2 to 44.4 °C – phase-crystal I; above 44.4 °C – liquid phase*

Gaseous IrF_6 was flown bottom-up (from 5th to 1st layer, general height 2 cm) through the fine (1 m) layers of UO_2F_2 granules in the vertical column (28 cm high and 1.2 cm inner diameter), at the rate of $V = 2$ cm/s at ~125 °C (see fig. 4).

The interaction IrF_6 with UO_2F_2 was suggested to be:

$$UO_2F_2 + 2IrF_6\,(gas) \rightarrow 2IrF_4 + UF_6 + O_2 \qquad (3)$$

with the formation of gaseous UF_6 and O_2 which volatilized during the experiment. After IrF_6 went through the column, the column contents were separated by five equal parts by height, so that five samples of IrF_6–UO_2F_2 interaction products were obtained: TNM-1 (grey powder), TNM-2 (grey powder with black inclusions), TNM-3 (grey powder with many black inclusions), TNM-4 and TNM-5 (practically black powders).

Figure 4. Schematic diagram of the sorption column filled with fine UO_2F_2

XPS spectra of the studied samples were measured with electrostatic spectrometers MK II VG Scientific, using non-monochromatized $AlK_{\alpha1,2}$ and MgK_α radiation under $1.3\ 10^{-7}$ Pa at room temperature. The device resolutions measured as full width on the half-maximum (FWHM) of the $Au4f_{7/2}$ line on the standard rectangular golden plate was 1.2 eV. Electron binding energies E_b(eV) were measured relatively to the binding energy of C1s electrons from hydrocarbons absorbed on the sample surface, accepted to be equal to 285.0 eV. For the gold standard, calibration binding energies E_b(C1s) = 284.7 eV and E_b($Au4f_{7/2}$) = = 83.8 eV were used. The full widths at half maxima (FWHM) in the tab. 1 are given relatively to that of the C1s line of hydrocarbons, accepted to be equal to 1.3 eV for comparison with the data of other studies. The uncertainty in determination of electron binding energies were ±0.2 eV and that of the relative line intensities was less than 10%.
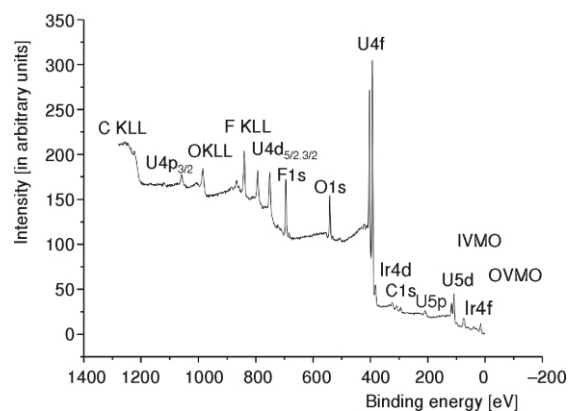
The studied samples were prepared as finely dispersed powders pressed in indium on titanium substrate (flat, thick layers with mirror surface). The powders were not ground to keep the surface intact. For all the samples, the valence band (0-50 eV), U4f-5d, Ir4f, O1s, F1s, and C1s spectra were measured. To avoid sample charging which can be really significant (up to 12 eV and stable in time), the calibration was done for each spectrum. It helped reduce the uncertainty in the binding energy determination down to 0.1 eV.

For all the samples, quantitative elemental and ionic analysis was done. It was based on the fact that the spectral intensity is proportional to the number of certain atoms in the studied sample. The following ratio was used: $n_i/n_j = (S_i/S_j)(k_j/k_i)$, where n_i/n_j is the relative concentration of the studied atoms, S_i/S_j – the relative core-shell spectral intensity, and k_j/k_i – the relative experimental sensitivity coefficient. The following coefficients relative to carbon were used in this work: 1.00 (C1s), 2.64 (O1s), 4.00 (F1s), and 15.8 ($Ir4f_{7/2}$) [6]. For uranium, the coefficients 26.51 ($U4f_{7/2}$) and 2.95 ($U5d_{5/2}$) were obtained taking into account the values for UO_2F_2, theoretical photoemission cross-sections [7], and kinetic binding energies.

RESULTS AND DISCUSSION

The XPS spectra of the valence and core electrons of UO_2F_2 (TNM-0) and five products of UO_2F_2-IrF_6 interaction (TNM-1, TNM-2. TNM-3, TNM-4, and TNM-5) were studied in the binding energy range 0-1000 eV. Only peaks attributed to the included elements were observed (fig. 5). This binding energy range can be subdivided into three subranges: outer valence molecular orbitals (OVMO) range, 0-13 eV, inner valence molecular orbitals (IVMO) range, 13-50 eV, and core electron range, 50-1000 eV [4]. Fine XPS structure parameters were also used. Since these parameters characterize various properties of the compounds, they are used together with traditional parameters like electron binding energies, chemical shifts and peak intensities [3, 4]. To simplify the discussion, both molecular and atomic terms are used in this work.
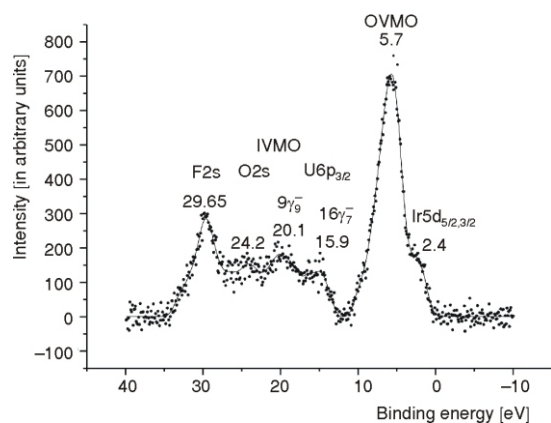
Low binding energy (0-50 eV) XPS. Valence electronic configurations for the basic state of atomic U and Ir are: $^{92}U6s^26p^65f^36d7s^2\ ^5L_6^0$ and $^{77}Ir5d^76s^2\ ^4F_{4-1/2}$. One can see that uranium and iridium can exhibit different oxidation states in compounds. Indeed, uranium (UO_2, UO_2F_2, *etc.*) and iridium (K_2IrCl_6, K_3IrCl_6, *etc.*) compounds of different oxidation states are known [3, 4].

Figure 5. Survey XPS from the TNM-5 sample

In the binding energy range 0-13 eV, the XPS from the studied samples (TNM-0 – TNM-5) exhibits the structure attributed to the OVMO electrons formed from the U6p,5f,6d,7s, Ir5d,6s, O2s, and F2s valence atomic shells (fig. 6). At the low binding energy ($E_b = 2.4$ eV), an intense Ir5d peak was observed as a shoulder. Its intensity is proportional to the iridium concentration on the sample surface. This peak is absent in the XPS from UO_2F_2 (TNM-0). The Ir5d relative intensity measured as the ratio of the intensities [I(Ir5d)/I(Ir4f$_{7/2}$)] must be proportional to the number of Ir5d electrons not participating in the chemical bond and must characterize iridium oxidation state (valency) in compounds. However, this is a topic of a special study and development of a technique for the determination of iridium valency in compounds on the basis of Ir5d relative intensity. In this work, the ratio [I(Ir5d)/I(Ir4f$_{7/2}$)] was measured to be 0.106 (constant) for all the studied samples, as expected. It indicates that the iridium oxidation state was constant. The calculated [I(Ir5d)/I(Ir4f$_{7/2}$)] was: 0.144 for Ir^{2+}, 0.125 for Ir^{3+}, and 0.105 for Ir^{4+} [7]. However, due to the high experimental uncertainty, this ratio can not unambiguously point out the iridium oxidation state (Ir^{3+} or Ir^{4+}). Also, the Ir4f relative intensities were measured [I(Ir4f)/I(Ir4f$_{7/2}$)] to characterize iridium contents in the samples (tab. 1). Despite the high measurement uncertainty, these values agree qualitatively with those of iridium contents on the basis of the [I(Ir5d)/I(Ir4f$_{7/2}$)] ratio (tab. 1).

The second binding energy range (13-50 eV) exhibits the structure attributed to the IVMO electrons related to the low binding energy filled U6p and O(F) shells. The parameters of this structure correlate with uranium close environment structure parameters in UO_2F_2 (interatomic distance uranium-ligand in axial and equatorial directions) [4]. The peaks at 14.9 and 20.1 eV (TNM-5) were attributed not to the atomic U6p$_{3/2}$ shells, but to the 16 $_7^-$ and 9 $_9^-$ IVMOs for the $[(UO_2)F_6]^{10-}$ (D_{6h}) cluster

Figure 6. XPS of the valence electrons from the TNM-5 sample

[8] (see also tab. 1, fig. 6). The OVMO-core binding energy differences characterize the interatomic distances, uranium-oxygen in the axial direction and uranium-fluorine in the equatorial plane. For UO_2F_2 (TNM-0), these interatomic distances are: $R_{U-O} = 0.174(2)$ nm and $R_{U-F} = 0.243(2)$ nm [4]. Also, it was shown that the 16 $_7^-$ and 9 $_9^-$ IVMO binding energy differences also correlate with the interatomic distance in the uranyl group UO_2^{2+} (see for example [4]). As a certain approximation, one can consider that, for example, the increase in the 16 $_7^-$ and 9 $_9^-$ IVMO binding energy differences indicates that the distance R_{U-O} in the uranyl group in UO_2F_2 decreases.

The following empirical expression based on O1s binding energy enables us to evaluate the interatomic distance R_{U-O} [9]:

$$R_{U-O} = 2.27 (E_b - 519.4)^{-1} \text{ [nm]} \qquad (4)$$

Indeed, taking into account the O1s binding energy 532.4 eV (tab. 1), one can evaluate the uranium-oxygen distance on the basis of expression (4) as $R_{U-O} = 0.175$ nm, which agrees satisfactorily with the value 0.174(2) nm [4].

Core electron spectra (50-1000 eV). The third binding energy range above 50 eV exhibits the core electron structure. Core electrons participate weakly in core molecular orbitals (CMO) formation. However, the structure related to the spin-orbit interaction (E_{sl}, eV), multiplet splitting (E_{ms}, eV), many-body perturbation *etc.*, can show up in this binding energy range [3-5]. These XPS structure parameters were taken into account.

Elemental and ionic XPS quantitative analysis usually employs the most intense peaks of the included elements [3-6]. In this work, the following peaks were chosen: U4f,5d, Ir4f, F1s, O1s, and C1s (tab. 1). The U4f,5d and Ir4f peaks were observed as spin-orbit split doublets with $E_{sl} = 10.8$, 8.6, and 3.0 eV, respectively ([3-5], figs. 7-9). The F1s, O1s, and C1s peaks were observed single and relatively sharp (figs. 10-12). The Ir4s,5s peaks at 95 eV and 691 eV, respectively, must widen as the number of the uncoupled electrons on an iridium ion grow (one extra uncoupled electron results in an 1 eV FWHM increase) due to multiplet splitting [4]. Unfortunately, these peaks were not observed in this work because of the low intensity.

The O1s and F1s spectra were always observed single and sharp at $E_b \sim 531.4$ eV and 685.7 eV, respectively (figs. 10 and 11). The C1s spectra from all the studied samples, except for TNM-4, were also observed single at $E_b = 285.0$ eV (fig. 12). The C1s spectrum from TNM-4 shows the CO_3^{2-}-related peak at 288.2 eV. The tab. 1 gives the calibrated FWHMs.

Data coming from other authors were taken into account in the discussion of the XPS from the studied

Table 1. Electron binding energies E_b (eV), peak full widths at half maxima (FWHM)[a] (eV), relative intensities[b] I(Ir5d)/I(U4f$_{7/2}$), relative concentrations[c] C(Ir/U) and IVMO binding energy differences 16 $_7^-$ − 9 $_9^-$ (ΔU6p$_{3/2}$, eV)

Sample	MO	I(Ir5d/I(U4f$_{7/2}$)	C(Ir/U)	ΔU6p$_{3/2}$	U5f$_{7/2}$	U5d$_{5/2}$	Ir4f$_{7/2}$	F1s	O1s	C1s
TNM-0 (UO$_2$F$_2$)	5.9 (2.6) 15.6 20.1 24.9 30.1	–	–	4.5	383.3 (1.4)	99.2 (1.4)	–	685.3 (1.1)	532.4 (1.3)	285.0 (1.3)
TNM-1	2.6 6.3 (2.1) 15.5 20.1 24.9 30.3	0.003	0.03	4.6	383.8 (1.3)	99.4 (1.4)	62.4 (1.3)	685.7 (1.0)	532.6 (1.3)	285.0 (1.3)
TNM-2	2.6 6.0 (2.1) 15.3 20.0 25.0 30.2	0.006	0.10	4.7	383.5 (1.3)	99.2 (1.2)	62.4 (1.3)	685.7 (0.8)	532.4 (1.3)	285.0 (1.3)
TNM-3	2.6 6.2 (2.2) 15.9 20.5 24.4 30.3	0.005	0.07	4.6	383.6 (1.4)	99.2 (2.0)	62.4 (1.2)	685.9 (0.9)	532.4 (1.3)	285.0 (1.3)
TNM-4	2.6 6.2 (3.1) 16.2 20.2 24.8 30.2	0.014	0.23	4.0	383.3 (1.5)	98.9 (1.7)	62.8 (1.4)	685.7 (1.6)	532.2 (1.7)	285.0 (1.3) 288.2
TNM-5	2.4 5.7 (2.3) 15.9 20.1 24.2 29.7	0.007	0.11	4.2	383.1 (1.3)	98.8 (1.3)	62.7 (1.3)	685.1 (0.9)	532.1 (1.3)	285.0 (1.3)
Ir [3, 5]							60.3			
IrCl$_3$ [3]							62.7			
K$_3$IrCl$_6$ [3]							62.7			
K$_2$IrCl$_6$ [3]							63.9			

[a] FWHM are given in parentheses; [b] relative intensities are given as the Ir5d/U4f$_{7/2}$ intensity ratios; [c] for comparison, the atomic concentrations Ir/U are given

samples. Thus, for UO$_2$, UF$_4$, -UO$_3$ and UO$_2$F$_2$, the U4f$_{7/2}$ binding energies are 380.9, 382.7, 382.4, and 383.4 eV, respectively [4]. For Ir, IrCl$_3$, K$_3$IrCl$_6$, and K$_2$IrCl$_6$, the Ir4f$_{7/2}$ binding energies are 60.3, 62.7, 62.7, and 63.9 eV, respectively [3].
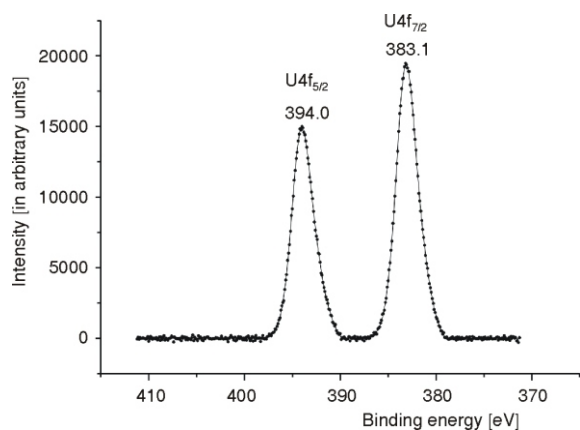

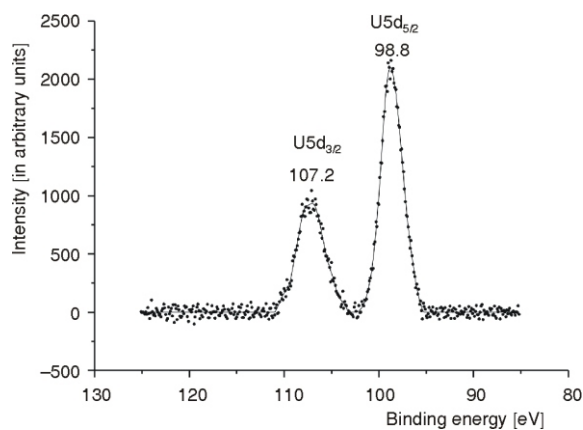**Figure 7. The U4f XPS from the TNM-5 sample**

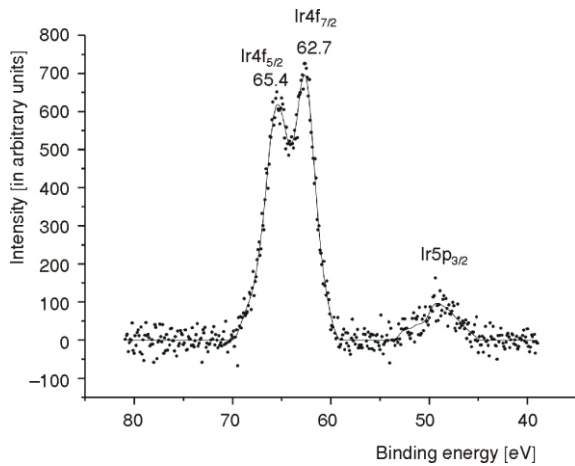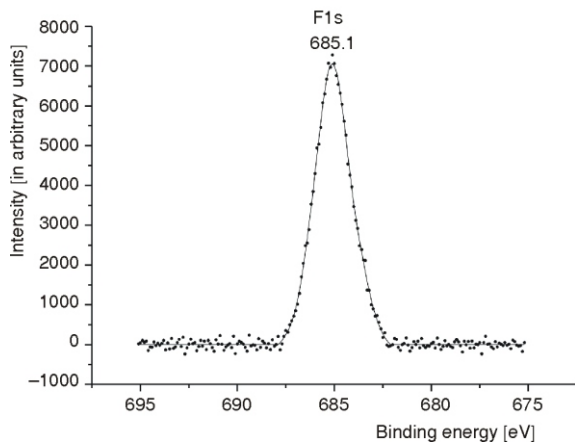**Figure 8. The U5d XPS from the TNM-5 sample**

Figure 9. The Ir4f XPS from the TNM-5 sample
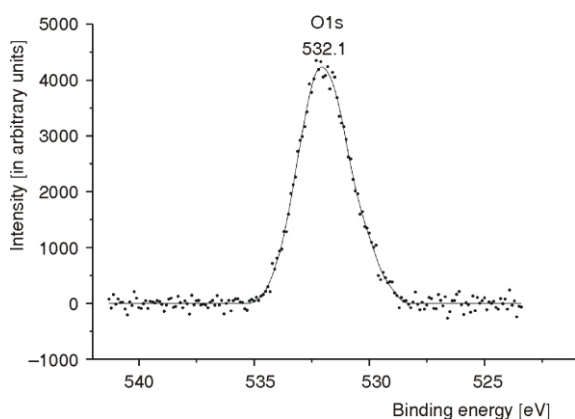

Figure 10. The F1s XPS from the TNM-5 sample

Figure 11. The O1s XPS from the TNM-5 sample

Sample UO_2F_2 (TNM-0). In UO_2F_2 (TNM-0) uranium ion presents as U^{6+}. Indeed, the OVMO XPS does not exhibit the U5f peak at zero binding energy. The U4f spectrum shows a doublet of the two sharp
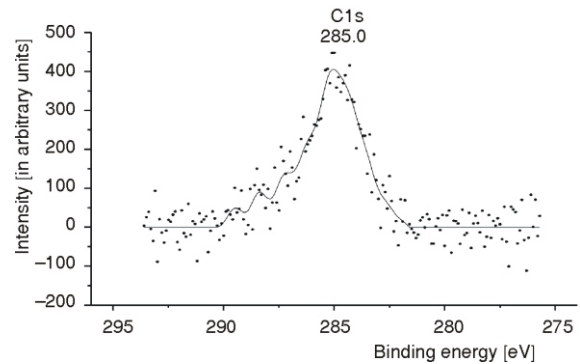

Figure 12. The C1s XPS from the TNM-5 sample. The solid line is a result of a 5-point smoothing of experimental data applied 200 times

peaks (tab. 1), without the shake up satellites. It can be explained by the violated long-range order and the fact that the satellites at 3.5 eV on the higher binding energy side are low intense due to the restricted spectrometer resolution. The $16_7^- - 9_9^-$ OVMO spectrum exhibits the two 4.5 eV distant peaks. A small amount of the saturated hydrocarbons was observed on the surface of the initial sample (tab. 1). It has to be noted that parameters of all measured in this work XPS coincide with the data for UO_2F_2 [4].

Sample TNM-5. The XPS survey from the TNM-5 sample, beside the UO_2F_2 related peaks, exhibits iridium peaks (fig. 5). The Ir5d peak was observed at $E_b = 2.4$ eV, the low intense Ir5p$_{3/2}$ peak – at E_b 50 eV and the Ir4f$_{7/2}$ one – at 62.7 eV (figs. 6 and 9). Spin-orbit splitting was E_{sl}(Ir4f) = 3.0 eV. Since the spin-orbit splitting is E_{sl}(Ir5p) 15 eV, the second component – the Ir5p$_{1/2}$ peak – overlapses with the Ir4f peak (fig. 9). Going from UO_2F_2 (TNM-0) to the TNM-5, one can see a significant narrowing of the peak in the F1s and F2s binding energy range (5_8^- $-^{15}_7$ IVMO), as well as the decrease of the 16_7^- and 9_9^- IVMO binding energy difference (tab. 1, figs. 6 and 10). This can be explained by the rise of the chemical equivalence of fluorine ions and the decrease of the U-O interatomic distance in the uranyl group on the surface. The XPS of other electronic shells did not change significantly (figs. 7, 8, and 11).

Sample TNM-4. Ir concentration in this sample is the highest. Indeed, the Ir5d intensity for this sample is about twice as high and the $16_7^- - 9_9^-$ IVMO binding energy difference is noticeably less than those in the spectra from the TNM-5 sample (tab. 1). Unlike the TNM-5, the TNM-4 sample contains more oxygen, fluorine, iridium, and carbon on the surface (see the elemental composition).

Samples TNM-3, TNM-2, and TNM-1. Going from TNM-3 to TNM-2 and TNM-1, one can observe the increase of oxygen and fluorine concentration and a decrease of iridium concentration (see the elemental

composition). The Ir4f spectra from the TNM-2 and TNM-3 samples at the lower binding energy exhibit an extra complex structure, possibly due to the overlapping with the iridium-related doublets. Since the similar extra structure was observed in the XPS from uranium and other elements, it was attributed to the heterogeneous charging of the samples. Since these samples contained some black inclusions (conglomerates), one can suggest that they are responsible fot this effect. Taking into account that the iridium XPS from the TNM-1 sample exhibits a normal structure, we did not make any special conclusions on the basis of the presense of iridium in other oxidation states in the TNM-2 and TNM-3 samples.
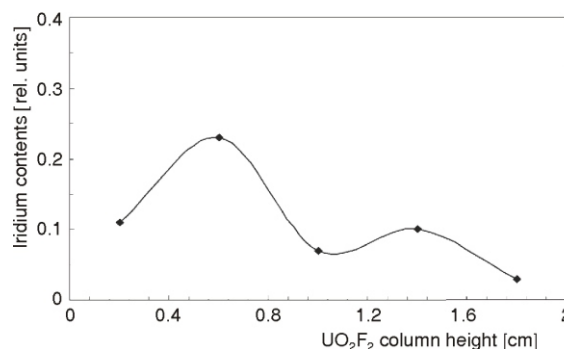
Quantitative analysis results. The uncertainty in peak intensities during the XPS quantitative elemental analisys of the studied samples was increased due to the multiplet splitting, many-body perturbation and the dynamic effect related extra structure. While the many-body perturbation effect results in the shake up satellites on the higher binding energy side from the basic peaks, the intensity of such satellites can be partially taken into account. The dynamic effect can not be taken into account, but its influence is negligible. All these effects can increase the uncertainty of the XPS quantitative analysis up to more than 10%. In this approximation, the quantitative XPS elemental and ionic analysis of the surface (~5 nm) of the studied samples relative to one uranium atom yielded the following:

$$U_{1.00}O_{1.97}F_{2.33}C_{0.41} \qquad \text{(TNM-0)}$$
$$U_{1.00}O_{2.09}F_{2.17}Ir_{0.03}C_{0.69} \qquad \text{(TNM-1)}$$
$$U_{1.00}O_{1.85}F_{2.11}Ir_{0.10}C_{0.28} \qquad \text{(TNM-2)}$$
$$U_{1.00}O_{1.61}F_{1.90}Ir_{0.07}C_{0.37} \qquad \text{(TNM-3)}$$
$$U_{1.00}O_{2.90}F_{2.53}Ir_{0.23}C_{0.91+0.14} \qquad \text{(TNM-4)}$$
$$U_{1.00}O_{2.14}F_{1.95}Ir_{0.11}C_{0.63} \qquad \text{(TNM-5)}$$

The data for the sample surface can slightly differ from those for the volume, since the XPS data reflect the sample composition from 5-10 nm depth. Figure 13 shows the iridium non-volatile compound distribution in relative to uranium along the UO_2F_2 layer in the column.

According to the Ir4f binding energy, the iridium oxidation state was suggested to be close to Ir^{3+} (tab. 1) [3]. The authors of [10] point out that IrF_3 and IrF_4 can exist, and the authors of [11] state that iridium trifluoride IrF_3 (black) can be synthesized by the reduction of IrF_6 with metallic iridium at 50 °C. IrF_3 (slightly distorted ReO_3 crystal structure) is relatively inert to water.

In conclusion, we'd like to note that the considered results showed that the XPS proved to be an effective tool for studying the elemental and ionic surface composition of various compounds.

Figure 13. Contents of non-volatile iridium compound spread along the UO_2F_2 column height measured as the ratio of the number of iridium atoms to the number of uranium atoms in the surface (5-10 nm) layer

CONCLUSIONS

The model reaction of the interaction of gaseous IrF_6 with fine UO_2F_2 in the sorption column revealed the change of color of the sorption column contents from pale-yellow to grey and black, indicating the formation of products of such an interaction.

The XPS study showed that the interaction of gaseous IrF_6 with fine UO_2F_2 at 125 °C results in the formation of stable iridium compounds where the iridium oxidation state is close to Ir^{3+}.

The distribution of a non-volatile iridium compound along the UO_2F_2 column height was established.

The highest Ir saturation of the sorbent (UO_2F_2), measured as the ratio of the number of Ir to U atoms, was shown to be 23%. It has to be noted that this ratio (Ir/U) was found for the surface (5-10 nm) layer of the samples.

ACKNOWLEDGEMENTS

REFERENCES

[1] Amano, D., Kawamura, F., Fukasawa, T., Takahashi, M., Sasahira, A., Shibata, Y., Ymashita, J., New Reprocessing Technology, Fluorex, For LWR Fuel Cycle-Hybrid Process of Fluoride Volatility and Solvent Extraction, International Conference Back-End of the Fuel Cycle, Global, Paris, September, 2001, R-No 015

[2] Rakov, E. G. , Tumanov, Yu. N., Butylkin, Yu. P., Tsvetkov, A. A., Veleshko, N. A., Poroikov, E. P., Basic Properties of Organic Fluorides, Textbook (in

Russian), (Ed. by N. P. Galkin), Atomizdat, Moscow, 1975

[3] Nefedov, V. I., X-Ray Photoelectron Spectroscopy of Chemical Compounds (in Russian), Khimiya, Moscow, 1984

[4] Teterin, Yu. A., Teterin, A. Yu., The Structure of X-Ray Photoelectron Spectra of Light Actinide Compounds, *Russian Chemical Reviews, 73* (2004), 6, pp. 541-580

[5] Fuggle, J. C., Martensson, N., Core-Levels Binding Energies in Metals, *J. Electr. Spectr. Relat. Phenom., 21* (1980), pp. 275-281

[6] ***, Practical Surface Analysis by Auger and X-Ray Photoelectron Spectroscopy (Eds. D. Briggs, M. P. Seah), John Wiley & Sons Ltd., New York, 1983

[7] Band, I. M., Kharitonov, Yu. I., Trzhaskovskaya, M. B., Photoionization Cross Section and Photoelectron Angular Distributions for X-Ray Line Energies in the Range 0.132-4.509 keV, Targets: 1 Z 100, *Atomic Data and Nuclear Data Tables, 23* (1979), pp. 443-705.

[8] Utkin, I. O., Teterin, Yu. A., Terehov, V. D., Ryzhkov, M. V., Teterin, A. Yu., Vukchevich, L., X-Ray Spectral Studies of the Electronic Structure of Uranyl Fluorite UO_2F_2, *Nuclear Technology & Radiation Protection, 19* (2002), 2, pp.15-23

[9] Sosulnikov, M. I., Teterin, Yu. A., XPS Study of Calcium, Strontium, Barium and Their Oxides (in Russian), *DAN SSSR, 317* (1991), 2, pp. 418-421

[10] Wells, A., Structural Inorganic Chemistry (in Russian) (Ed. M. A. Poray-Koshts), Mir, Moscow, 1987

[11] Cotton, F., Wilkinson, G., Advanced Inorganic Chemistry (in Russian) (Ed. M. E. Dyatkina), Mir, Moscow, 1969

Владимир Н. ПРУСАКОВ, Јуриј А. ТЕТЕРИН, Николај М. ТРОЦЕНКО,
Константин И. МАСЛАКОВ, Антон. Ј. ТЕТЕРИН, Кирил Е. ИВАНОВ,
Филип С. БОЧАГИН, Дмитриј В. УТРОБИН

ИСТРАЖИВАЊЕ РЕНДГЕН-ИНДУКОВАНОМ ФОТОЕЛЕКТРОНСКОМ СПЕКТРОСКОПИЈОМ ПРОИЗВОДА ИНТЕРАКЦИЈЕ ГАСОВИТОГ IrF₆ СА ЧИСТИМ UO₂F₂

При репроцесирању нуклеарног горива флуоризацијом, сувим методом регенерације ислуженог нуклеарног горива, за сепарацију плутонијума из гасовите смеше употребљава се уранилфлуорит (UO_2F_2). Пошто плутонијум захтева посебан поступак, као термодинамички модел плутонијумхексафлуорида (PuF_6) користи се иридијумхексафлуорид (IrF_6). Моделована интеракција гасовитог IrF_6 са чистим UO_2F_2 у сорпционој колони указала је на промену боје садржаја сорпционе колоне од жуте до сиве и црне, назначујући настајање производа такве интеракције. Истраживање рендген-индукованом фотоелектронском спектроскопијом показује да интеракција гасовитог IrF_6 са чистим UO_2F_2 на 125 °C доводи до настајања стабилних иридијумских једињења у којима је стање иридијумске оксидације блиско Ir^{3+}. Установљена је зависност елементарног састава слојева у сорпционој колони од дебљине продирања IrF_6.

Кључне речи: *рендген-индукована фотоелектронска спектроскопија, уранилфлуорит,
иридијумхексафлуорид, технологија издвајања актинида из гасне смеше*